Regular Article

PHYSICAL CHEMISTRY RESEARCH
Published by the
Iranian Chemical Society
www.physchemres.org
info@physchemres.org

Phys. Chem. Res., Vol. 8, No. 3, 543-556, September 2020
DOI: 10.22036/pcr.2020.222756.1742

Functionalized Single-atom Thickness Boron Nitride Membrane for Separation of Arsenite Ion from Water: A Molecular Dynamics Simulation Study

N.S. Tabrizi[a], B. Vahid[a,*] and J. Azamat[b]

[a]*Department of Chemical Engineering, Tabriz Branch, Islamic Azad University, Tabriz, Iran*

[b]*Department of Basic Sciences, Farhangian University, Tehran, Iran*

(Received 8 March 2020, Accepted 28 May 2020)

In this research, the performance of functionalized boron nitride nanosheet (BNNS) as a nanostructure membrane with single-atom thickness for the separation of arsenite (AsO_3^{3-}) ions from aqueous solution was examined by molecular dynamics simulation method. The simulated system included a functionalized BNNS placed in an ionic solution containing sodium arsenite, while the external pressures were applied to the system. For the high-water permeability and full ions rejection, the pore of BNNS was functionalized by passivizing pore edge atoms with F and H atoms, then hydrostatic pressures in the range of 5-100 MPa were applied to the system. During the molecular dynamics simulations, water molecules and arsenite ions were monitored, and some analyses such as water flux, the density profile of water and ion, hydrogen bonds, and radial distribution function were performed. Results showed that functionalized BNNS was able to conduct water molecules with high permeability through its pore, whereas AsO_3^{3-} ions were not able to pass through the pore.

Keywords: Boron nitride nanosheet, Functionalized membrane, Arsenite, Molecular dynamics simulation

INTTRODUCTION

Water pollution by arsenite (arsenic III) is considered as one of the most significant environmental issues, due to toxicity and the tendency of arsenic to bioaccumulation and sustainability in nature [1]. It is necessary to remove arsenic pollutants from aqueous solutions to safeguard the environment and prevent them from entering the body tissues by the food chain as biodegradable contaminants. During the extraction, because of the nature of mineralogy and the formation of gold deposits, wastewater containing arsenic is introduced into the environment [2]. The concentrations of some metals such as copper, zinc, aluminum, arsenic, manganese and iron, increase in low pH aqueous solution. Metal ions are being discharged into the water with more than the authorized concentration by industrial activities, and thus they cause many problems for human health and environmental issues [3].

*Corresponding author. E-mail: behrouz_vahid@iaut.ac.ir

Purifying the effluent before discharging makes it possible to reduce the undesirable effects of heavy metals pollution [4]. Depending on their toxicity and standard depletion, the removal of arsenic from the wastewater by the processing plant before being released is essential. This matter is vital because arsenic does not disappear; however, its composition is changeable. The United States Environmental Protection Agency (EPA) declined the maximum amount of arsenic of water from 0.05 mg l^{-1} to 0.01 mg l^{-1} [1]. Also, according to the EPA indexes, arsenic is a substance causing cancer even *via* its low concentrations in drinking water.

Arsenic can infect groundwater in two ways; firstly, through air contacts such as chemical weathering of arsenic, including sulfide minerals, and secondly from human-made pollution such as uncontrolled wastewater from mining and metallurgy as well as the use of organic alloys containing arsenic and pesticides. Arsenic has two primary forms of arsenate (As^{5+}) and arsenite (As^{3+}) in soil and natural waters. The As^{3+} species has more mobility in groundwater

than As^{5+} and is 25 to 60 times more toxic. The concentration of arsenic species in water largely depends on the two factors of redox potential and pH. In low pHs and under moderate thermodynamic conditions, As^{3+} has much more stability, and is found in molecular structures such as AsO_3^{3-}, H_3AsO_3, $H_2AsO_3^-$ and $HAsO_3^{2-}$. Under high oxidation, As^{5+} is the dominant state and found in H_3AsO_4, $H_2AsO_4^-$, $HAsO_4^{2-}$, and AsO_4^{3-} molecular structures [5].

The primary processes for removing arsenic are adsorption, coagulation, and freezing [6]. In 2005, EPA introduced several ion-exchange methods, active alumina, membrane filtration (reverse osmosis, nanofiltration and electrodialysis), coagulation (modified filtering and softening) for removing arsenic. These methods require the additional materials, otherwise they show no selectivity and need frequent modifications; moreover, most of them are expensive and generate secondary wastes [7]. In addition to methods mentioned, other novel processes have been introduced to apply the nonstructural materials in ion separation. For instance, nanostructure membranes like boron nitride nanosheet (BNNS) properly was applied for this purpose. Some studies have investigated the role of the electronic structure of the BNNS and the effect of atomistic details of the BNNS surface area on the dynamical interactions between nanosheet-ion (As^{3+}) and nanosheet-water in aqueous solutions using molecular dynamics (MD) simulation [8]. We focused on the effects of the factors influencing on separating water molecules from arsenite ions, such as the effect of chemical groups used to functionalize the BNNS, and determining the appropriate size for drilled pore on the BNNS and the ability of this membrane in separation of ion-water due to the unique specifications of this nanosheet. The BNNS membrane contains boron and nitrogen atoms linked together *via* a covalent σ-bond. The unique specifications of BNNS possesses include electrical insulation, wide energy gaps, UV photoluminescence, excellent chemical and thermal conductivity, and stability [9].

Furthermore, its structure is analogous to graphene; however, there are some differences. For instance, the thermal and chemical strength of the BNNS is more than those of graphene, which can be appropriately recovered after burning or heating without oxidization [10]. Moreover, its tensile strength and Young's modulus are 102 GPa and 145 GPa, respectively. As a consequence, the BNNS has the appropriate resistance in severe operational conditions. A pristine BNNS is impermeable to ions because the electron density of its aromatic rings suffices to reject ions; hence, it can be a capable membrane in the process of water treatment.

Recently, researchers have theoretically studied the separation of mercury and copper ions, as the heavy metals, from aqueous solutions by the BNNSs using MD simulation. They simulated a box containing a boron nitride sheet and an ionic solution of mercury chloride and copper chloride. By applying an external voltage to the system, the mercury and copper ions were able to cross through the pores of the membrane with a high efficiency. In another study, the separation of heavy metals from aqueous solutions was performed using the functionalized graphene and BNNSs. The researchers used the MD to investigate the separation of Zn^{2+} ion into an aqueous solution by applying an external voltage to the simulation box. Their results demonstrated that both nanostructures could separate zinc ions from aqueous solutions, and the BNNS has a better performance compared to graphene [11].

In an experimental study, Chen *et al.* [12] fabricated a membrane contained BNNS in its structure aiming at water purification. BNNSs in the membrane's structure made membrane stable in acidic and basic environments and created nanochannels that facilitated the passage of molecules through the membrane with fast movements. This membrane could be selective to the molecule size. An essential characteristic of these nanochannels was their stable condition during the filtration process, which was not destroyed by passing the molecules. By increasing the size of molecules, they could not move across the membrane, while water molecules with an acceptable flow rate could pass across the membrane because of their smaller size. In other work, Jafarzadeh *et al.* [13] designed four different BNNSs with functionalized pores (two fluorinated BNNSs with different areas of the pore: one hydrogenated, and one hydroxylated). They showed that the fluorinated boron nitride nanosheet with 15.8 $Å^2$ pore area has a higher water flux compared to the other functionalized boron nitride nanosheets. They also calculated the potential of mean force values for water molecules in all the systems understudy. Based on the results, the water molecules encountered the

lower energy barrier at the fluorinated pore, and, consequently, could easily pass through the pore because of the higher hydrophilic nature of the functionalized pore.

In a DFT-based study, the adsorption of As(III) was performed using the boron nitride nanosheets and Fe_3O_4 functionalized boron nitride nanosheets, in which the latter showed a better performance, aligning with the experiment [14].

As far as we are aware, there is no investigation regarding the separation of AsO_3^{3-} (arsenic III) from water by a functionalized BNNS. In the present research, using the MD simulation, we studied the separation of AsO_3^{3-} from an ionic solution using the BNNS with a pore drilled on its center and functionalized with F and H atoms. Relying upon applying external pressure on the simulated system, we studied the mechanism of the separation process of ions from water. The obtained data can be applied to assist the design of nanostructured membranes for the removal of harmful contaminants from water sources.

METHOD AND SIMULATION DETAILS

Figure 1 displays a snapshot of the simulated system. The dimensions of the simulation box were $3 \times 3 \times 8$ nm^3, and the dimensions of the BNNS membrane were 3×3 nm^2. The box consisted of 2633 water molecules, and 10 AsO_3^{3-} and 30 Na^+ ions were dissolved in this aqueous solution.

The monolayer of BNNS was functionalized with both hydrogen (-H): 4 atoms, and fluorine (-F): 7 atoms, attached to the pore edge of the BNNS (see Fig. 2). The nitrogen atoms at the pore edge bonded on fluorine atoms and hydrogen atoms connected to boron atoms. Electronic structure and atomic geometry of the pore edges play a crucial role in treating water molecules in the systems, including biological molecules. Due to the larger electronegativity of fluorine atoms compared to the chlorine atoms, fluorine atoms have the more ability to increase the charge accumulated on the pore. Some authors suggested that fluorine termination could be a more plausible modulation route, since boron atoms are more electrophilic and may preferentially bind to the F atoms. Fluorinated pore exhibits a significantly reduced bandgap [15]. The atomic structure and the charge states of the pore rely on environmental circumstances, that have been identified as the major contributing factors for determining the energetics of the pore. The distance between the next-nearest-neighbor nitrogen and boron atoms decreases and increases, respectively, with the injection of excess electrons. Here, in the pore edges, due to the presence of more nitrogen atoms in comparison with the number of boron atoms, through doping with excess electrons, the electron chemical potential increases under nitrogen-rich and electron-rich environments on the structure of the pore edges [16].

The area of the created pore was about 13.15 $Å^2$ which was estimated by the number of benzene rings taken from the BNNS surface. The pore size was measured by showing atoms as van der Waals spheres and calculating the amount of area not filled by any atomic representations. The thorough geometric design of the functionalized BNNS was optimized using the density functional theory (DFT) method to attain atomic charges and their desired structures. The DFT procedure was carried out by the GAMESS-US package [17] at the B3LYP level of theory, applying 6-311G basis sets. To improve SCF convergence, we have implemented an efficient direct inversion of the iterative subspace (DIIS) algorithm, which can reduce the number of required SCF iterations in most calculations. In DFT calculations, an SCF convergence criterion of 10^{-5} and the standard 96-radial, 302-angular point integration grid was used. The partial charges obtained from DFT estimations for the functionalized membranes, and Lennard-Jones parameters of atoms obtained from reference [11] are presented in Table 1 (all CHARMM force field and Lennard-Jones parameters for all atoms are listed in Table S1 in Supporting Information).

For the water molecules, the TIP3P, TIP4P and SPC/E models were all used in the scientific literature. In this study, the TIP3P model [18] was utilized, which has a premier diffusion and structural properties over standard models and is thus more suitable for the study of water interactions in the systems including biological molecules [18]. It is worth noting that in this work, the water flow achieved from the TIP3P model is more significant than that from SPC/E or TIP4P model [19]. These different force fields may cause a slight difference in the simulation results. However, currently, no consensus has been reached on the most suitable force field for simulating the water

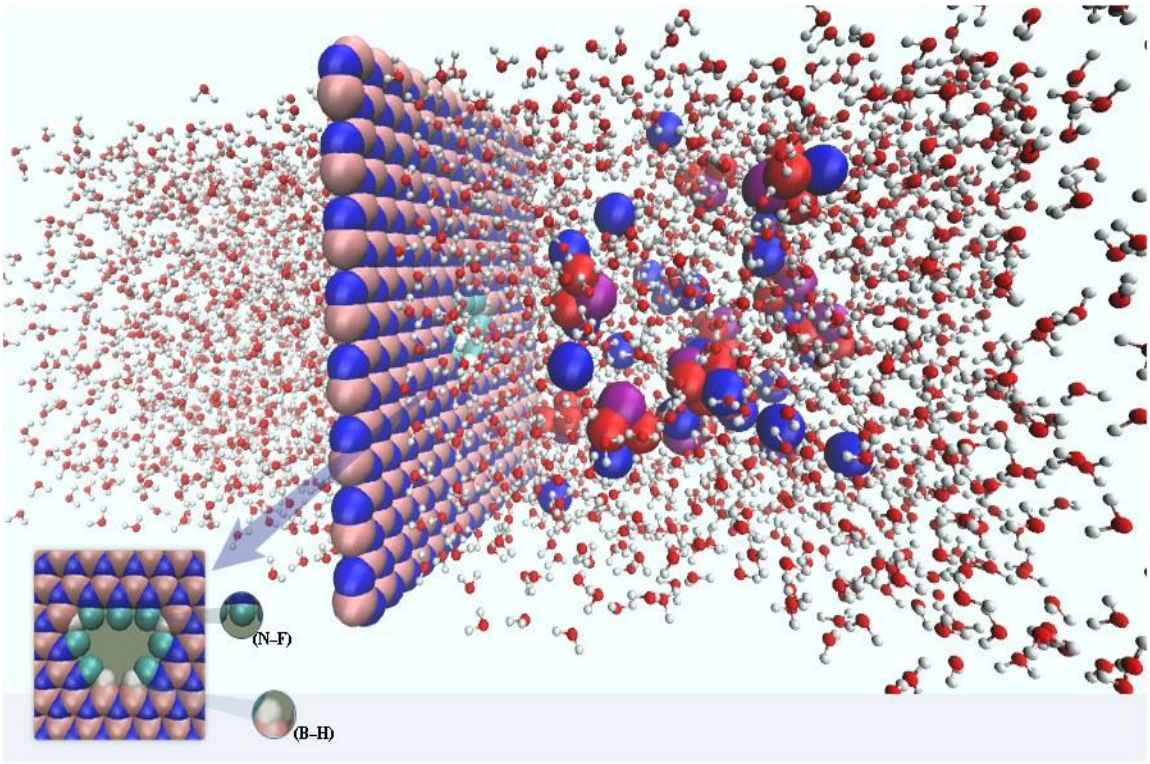

Fig. 1. A snapshot of the simulated systems including functionalized BNNS membrane immersed in aqueous solution of Na_3AsO_3 (red: O, white: H, blue: Na^+, Cyan: F and purple: As^{3+}).

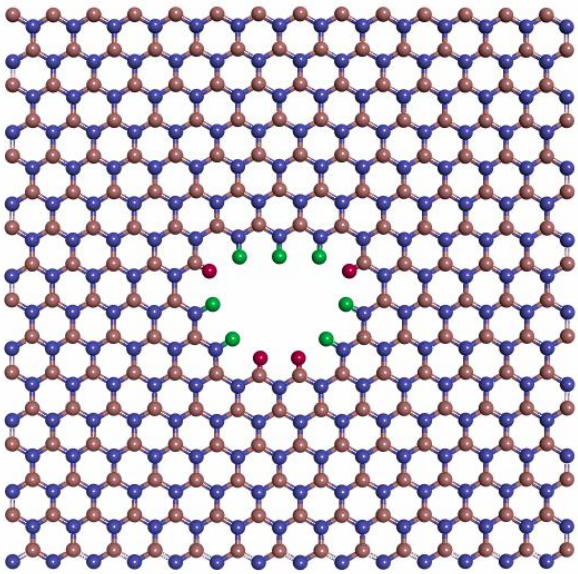

Fig. 2. Chemically functionalized BNNS membrane by hydrogen (-H) and fluorine (-F). Blue is nitrogen, brown is boron, red is hydrogen, and green represents fluorine.

Table 1. Partial Charges and Lennard-Jones Parameters for all Types of Atoms

Atom type	Partial charges obtained from DFT	σ (Å)	ε (Kcal mol^{-1})
Nitrogen	-0.40	1.00	0.669
Boron	0.40	3.45	0.397
Nitrogen bonded to fluoride	0.25	1.00	0.669
Boron bonded to hydrogen	0.05	3.45	0.397
Fluoride bonded to nitrogen n	-0.25	2.99	0.135
Hydrogen bonded to boron	-0.05	2.28	0.028
Sodium	+1.00	2.43	0.046
Oxygen	-1.34	3.47	0.135
Arsenic	+1.02	4.01	0.785

purification membranes. However, in this work, the TIP3P water model due to its success in modeling liquid water [20] was used. In comparison to other models, TIP3P has better structural and thermodynamic properties [20]. To further verify this statement, the diffusion coefficient of water molecules was calculated using the NVT ensemble, and good agreements were found with data available in the literature.

The BNNS membrane was placed in the center of the simulation box, and also for all runs, the atoms of BNNS membrane were restrained with a harmonic constraint to avoid the vertical movement of the membrane; although the functional groups on the edge pores of the membrane were permitted to be flexible. Also, water molecules and ions were allowed to move freely. We have to include the harmonic restraints in the force field in order to match the membrane dielectric constant with the experimental value. The errors raised from the harmonic restraint may affect the structure of the membrane during the simulation. However, simulations with no harmonic restraint will crumple the structure of the membrane. The applied force was performed on the water molecules in the z-direction of the system to comply with Eq. (1):

$$\Delta P = (n \,.\, F) / A \tag{1}$$

where n shows the number of water molecules, F indicates a fixed force in pN, A is the area of the system (m^2), and ΔP is the amount of applied pressure in Pa, which was in the range of 5-100 MPa. In general, force fields are the fundamental basic parameters in MD calculation, forming the equations for calculating the energy of molecules using the suitable parameters. Through potential energy function calculations, the amount of force is obtained by adding bonded and non-bonded potentials according to Eq. (2):

$$U = \sum U_{nonbonded} + \sum U_{bonded} \tag{2}$$

The MD method demonstrates the system activities using calculations of inter- and intramolecular interactions for all atoms by the force field parameters. The force fields are usually a combination of internal coordinates and terms describing a portion of potential energy.

The bonded potential comprises the bond length, bond angles, and dihedrals angle terms that involve interaction between all atoms bonded to each other by covalent bonds and is given by Eq. (3):

$$U_{bonded} = \sum_{bond} \frac{1}{2} k (r_{ij} - r_0)^2 + \sum_{angle} \frac{1}{2} k_\theta (\theta - \theta_0)^2 + \sum_{dihedral} k_\varphi (1 + \cos(n_\varphi - \delta) \quad (3)$$

where r_{ij} is the distance between atoms, r_0 is the equilibrium length bond, k is the spring constant, θ is the angle (radian) between three atoms, θ_0 is the equilibrium angle, and k_θ is the angle constant, -kφ is reciprocating rotational constant force. The current torsional angle is known as φ, -δ is the phase angle, and -n shows the periodicity.

Force fields also record electrostatic and van der Waals interactions to describe non-bonded interactions between atoms, known as long-range and short-range interactions. In this research, the Lennard-Jones potential and Coulomb potentials were applied for the determination of the van der Waals and electrostatic interactions, respectively [21], as Eq. (4):

$$U_{eff} = U_{vdw} + U_c = 4\sqrt{\varepsilon_i \varepsilon_j} \left[\left(\frac{\sigma_i + \sigma_j}{2r_{ij}} \right)^{12} - \left(\frac{\sigma_i + \sigma_j}{2r_{ij}} \right)^{6} \right] + \frac{q_i . q_j}{4\pi\varepsilon_0 r_{ij}} \quad (4)$$

where r_{ij} is spacing between the two particles -i and -j, ε_i and σ_i represent the Lennard-Jones parameters, and $-q_i$ and $-q_j$ are the partial charge in the CHARMM force field for the atoms -i and -j. For the calculations of the cross-interaction parameters, the Lorentz-Berthelot compounded rules were applied:

$$\varepsilon_{ij} = \sqrt{\varepsilon_i . \varepsilon_j} \quad and \quad \sigma_{ij} = \frac{\sigma_i + \sigma_j}{2} \quad (5)$$

where $-\varepsilon_{ij}$ and $-\sigma_{ij}$ intended as the Lennard-Jones parameters given to atoms -i.j. For calculating long-range electrostatic interactions, the particle mesh Ewald scheme (PME) [22] was used. The velocity Verlet integration method is used to advance the positions and velocities of the atoms in time [23].

The MD were performed using the NAMD2.12 [24] software with 12 Å cut-off and 1fs time step and visualized using VMD1.9.3 [25]. The pair list distance was selected 14 Å to speed up MD computations. The system was minimized at 0 K, by 50000-time steps and equilibrated with periodic boundary conditions by 20000-time steps and canonical (NVT) ensemble at 298 K. The Langevin thermostat was used to hold the temperature at 298 K. Eventually, to create the induced pressure, we applied an amount of pressure to the system along the z-direction at 298 K temperature during a simulation time of 5 ns. All of the results reported in this research were attained in an average set of 5-7 independent simulations from various initial velocity distributions.

RESULTS AND DISCUSSION

In the present research, we successfully designed a modified BNNS with a pore in its center for the separation of AsO_3^{3-} ions from aqueous solution. This study has tended to focus on the evaluation of the parameters such as the pore structure and the applied pressure amount that would allow the BNNS membrane to exhibit high water permeability while providing a complete rejection for ions. The study of these features is entirely feasible by assessing some analyses such as the water flux, the density profile, radial distribution function, and the number of hydrogen bonds during the simulation time.

Water Flux

Figure 3 indicates the water flux through the functionalized pore of BNNS. The water flux shows the number of passed water molecules through the functionalized pore of BNNS per 1 ns [26]. The number of water molecules transferred across the BNNS pore significantly increased due to the enhancement of the applied pressures.

As mentioned, one of the essential factors affecting the water permeation across the pore of the membrane is the chemical functionalization of the pore edge. In the BNNS membrane with an hourglass-shaped nanopore, water molecules permeate through it. The particular arrangement of hydrophilic atoms (fluorine atoms) in the pore leads to more propensities of water molecules. Notably, the formation of hydrogen bonds between water molecules and fluorine atoms at the edge pore increases the dynamics of the chain structure of water molecules passing through the pore of BNNS. This bonding takes place on each side of the membrane and causes to build the chain structure of water molecules inside the pore. The results showed that the number of water molecules passing through the pore

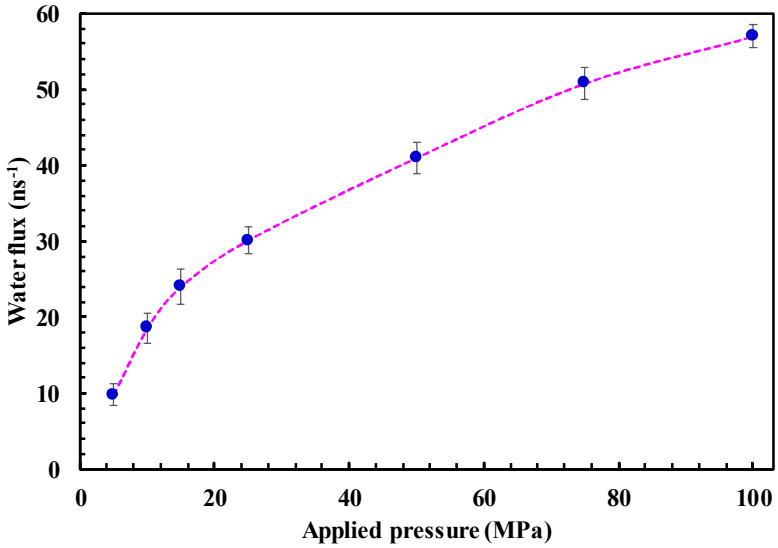

Fig. 3. The water flux as a function of used pressures. Each data point demonstrates the mean of 5-7 sets of independent simulations from diverse initial velocity distributions.

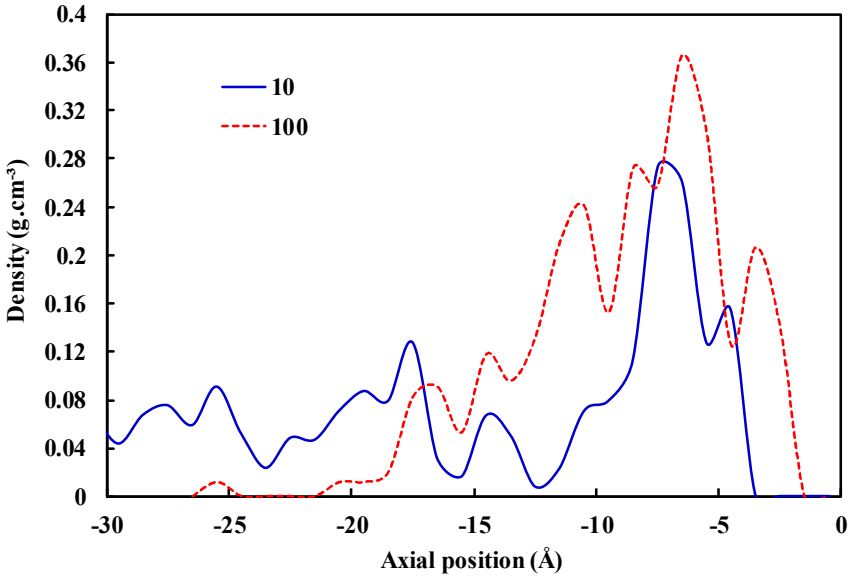

Fig 4. Arsenite (arsenic III) ions density profile under 10 MPa and 100 MPa pressures.

increased with the increment of pressure applied. However, this pressure increase did not affect passaging AsO_3^{3-} ions, and no ion passed through the pore because of the electrostatic interaction between the edge atoms of pore and ions. Figure 4 shows the density profile of AsO_3^{3-} ions under 10 MPa and 100 MPa pressures.

The zero point in Figure 4 on the x-axis is the location of the BNNS sheet. As can be seen, the ions are

accumulated at the one side (feed side) of the membrane in different applied pressures (low or high pressures), and they were not capable of passing through the pore. The peak intensity of the density profile of AsO_3^{3-} ions at the 100 MPa pressure near the BNNS was much more than that of the 10 MPa pressure, while by closing near the pore, both curves demonstrated a downward intensity to zero. Because of the existing repulsion force between the fluorine atoms (by a negative surface charge at the pore edge) with AsO_3^{3-} ions (which have two negative charges in oxygen atoms). When there is no way to cross the ions through the pore, they accumulate near the BNNS, causing an increase in the density of AsO_3^{3-} ions. By choosing the appropriate functional group for passivating the pore edge and determining the suitable size for the pore area, the BNNS membrane acted effectively as a filtration membrane for AsO_3^{3-} ions.

Water Structure Properties

To investigate the structure of water molecules in the simulated system, we considered the density profile of the water molecules in the simulation box in Fig. 5. There are two peaks on both sides of BNNS in the density profile plot, indicating the accumulation of water molecules and their propensity to localize in this area; see Figs. 5a and 5b. The peak of water density increases with pressure (feed side) and shifts toward the right side (pure water), which turns into more freshwater. As shown in the figure, arrangements of water molecules were not the same in all locations, and they accumulated close to the membrane owing to the non-bonded van der Waals interaction of water molecules and membrane atoms. Hence, the density of water in the layered structure was higher than that in the bulk water. Of course, it should be noted that water molecules can pass through the pore, contrary to the behavior of ions.

Radial Distribution Function

The radial distribution function (RDF) is the probability distribution of a particle at a determined distance from another particle that describes the structure of the water molecules. Figure 6 shows the RDF curve between water molecules at a distance of z = 3.5 Å from the membrane compared with their RDF in the entire system.

The peak intensity of the RDF inside the mentioned area shows an ascended trend compared with the whole system. It increased with increasing applied pressure because of the accumulation of water molecules at a certain distance from the BNNS (as can be seen in Fig. 5), due to the non-bonded interactions of water molecules with the membrane. Although BNNS has a hydrophobic nature because of the water molecule's contact angle (hydrophilic < 90° > hydrophobic) on the boron nitride's surface, studies showed that the bond between boron and nitrogen is polar and, consequently, could interact with water molecules. As shown in Fig. 6, the first peak in RDF curve is at 3 Å which indicates all the neighboring water molecules are at the distance of 3 Å with respect to each other. Also, the peak of the RDF curve in the region z = -3.5 Å is much higher than that of the RDF profile at all of the simulation system.

Figure 7 shows the arrangement of the water molecules surrounding AsO_3^{3-} ions, obtained from the trajectory files of the simulations. The first peak in the ion-water RDF correlates with the distribution of the first adjacent water molecules surrounding the ions (first hydration shell), indicating the formation of water molecules at the distance of 1.75 Å from ions. Also, this trend does not change by changing the pressure.

The first hydration shell around the ions destroys the structure of water molecules' hydrogen bonds network surrounding the ions and causes a reduction in the number of hydrogen bonds, which are continually breaking down and re-forming. Consequently, the hydrogen bond interaction between the water molecules is comparatively weak; furthermore, some of the interactions between water molecules and ions can also occur; see Figs. 8a and 8b. In these figures, the water network structure is seen as the formation of the first hydration shell around the ion.

The slight peak height on the right side of the first peak in the RDF curve shows the second hydration shell of ions taking place at a distance of 2.75 Å water molecules with ions (Fig. 7). This ascending trend is owing to the three positive charges in the valence shell of arsenite ions and their tendency to complete the hydration shells leading to the increased charge density of ions. Therefore, increasing the number of water molecules in the surrounding ions is expected.

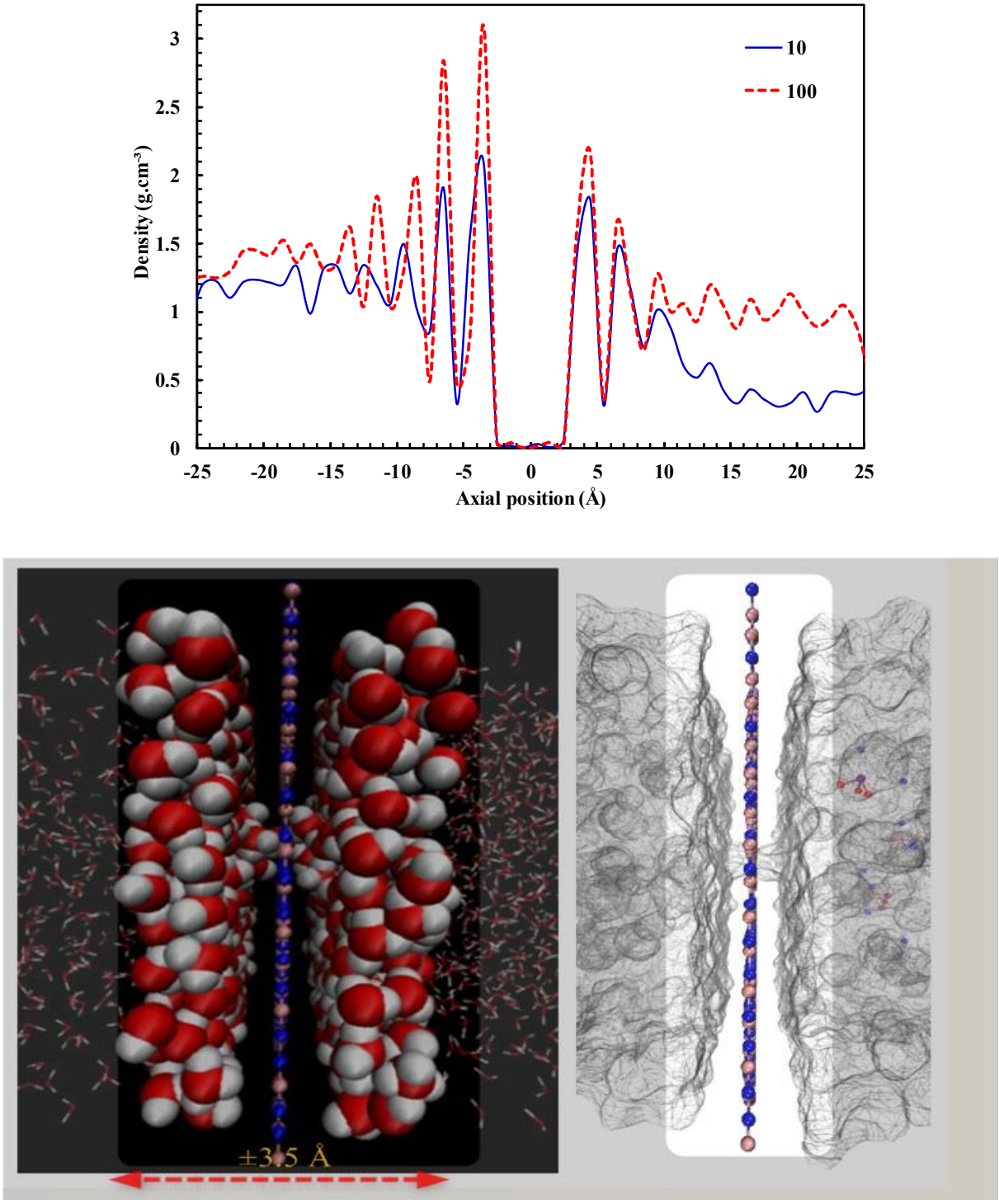

Fig. 5. (a) Density profile of water molecules under 10 MPa and 100 MPa pressures in simulation box, (b) Layered structure of water molecules on both sides of BNNS membrane.

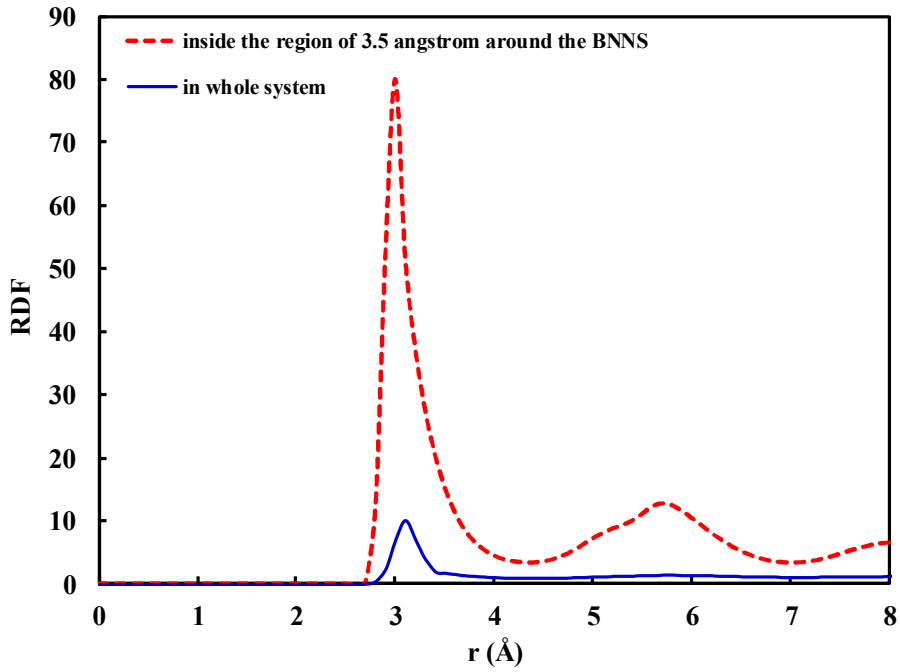

Fig. 6. RDFs of water molecules in the simulated system at 100 MPa pressure.

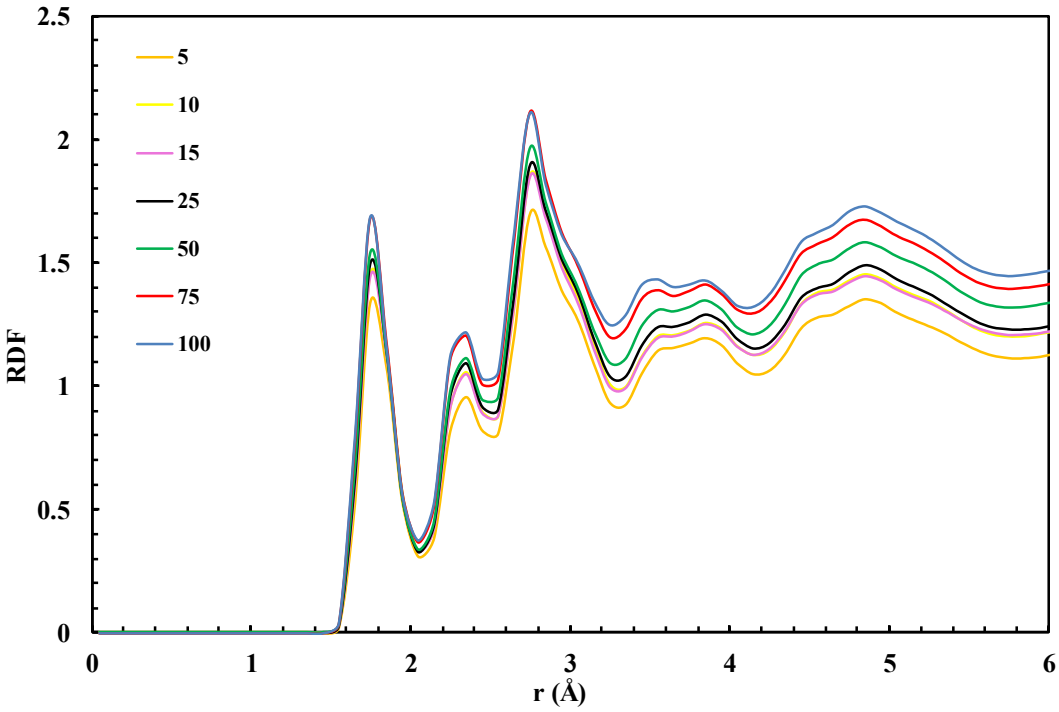

Fig. 7. RDF of ion-water in the simulation box under various applied pressures.

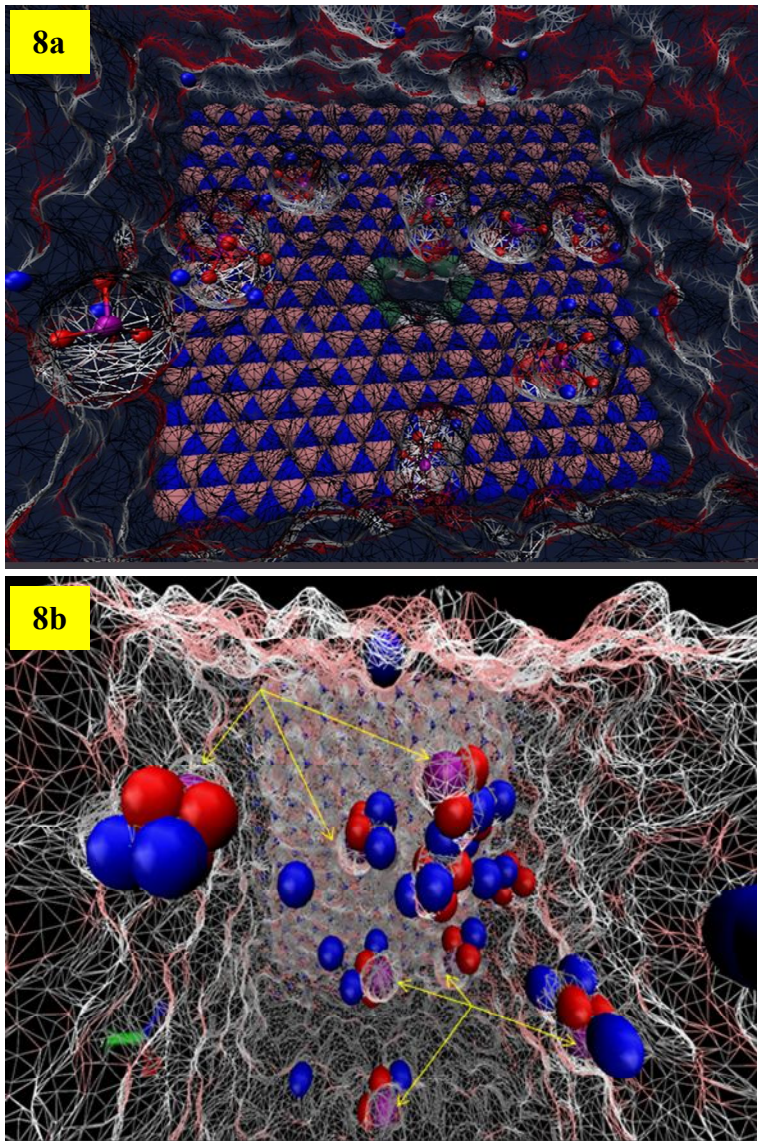

Fig. 8. (a,b) The snapshots of the simulated system showing the interaction between ions and water molecules. Purple: arsenite, blue: sodium and into the bulk structure around atoms, white: hydrogen, and red: oxygen atoms.

Hydrogen Bonds

When the hydrogen atom of the water molecule and the nonbonding electron pairs of electronegative atoms approach each other, a hydrogen bond is created [27]. Another critical parameter, for the number of hydrogen bonds of water molecules, is the pair dynamic of these bonds, which are performed by the VMD software during the simulation. At first, we define the H-bond for the software; donor-acceptor distance: 3 Å and angle cutoff: 20 degrees.

Due to the high electronegativity of the -F atom on the edge pore, a hydrogen bond was created between water

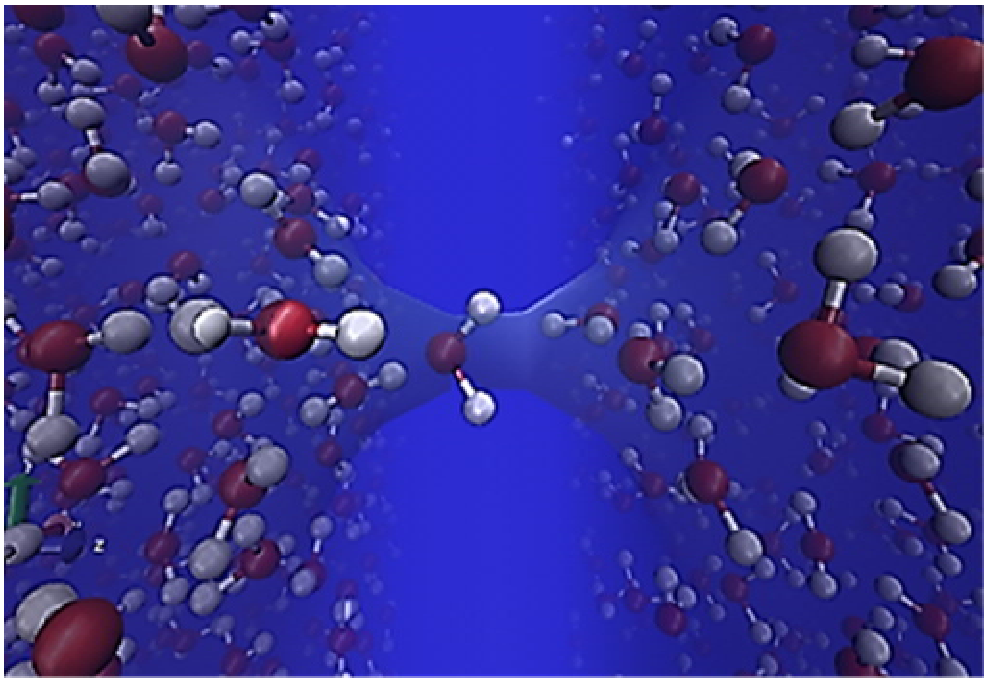

Fig. 9. A snapshot of orientation of water molecule when passing through the pore.

molecules and -F atoms on the edge pore when the water molecules want to pass through the pore. The water molecules have a particular orientation when approaching the functional pore, so they come close to the pore from the hydrogen atom's side. The geometry of the interaction site regulates the position of the interacting atom of the water molecule as an "acceptor" or a "donor" to minimize the steric interactions with covalently bound neighbors. So, orientation of water molecule to form hydrogen bond[28] leads to increase the water flux through the BNNS [29]. Consequently, the pair's dynamic of hydrogen bonds plays a dominant role in construction of water molecules as a single structure and passing through the pore with high flux. Figure 9 is a snapshot of the water molecule crossing through the membrane pore at 1.87 ns (in Fig. S1, the dipole orientation of a selected water molecule during the simulation time is presented).

Results of MD showed that the number of hydrogen bonds between water molecules in the whole system was not affected by increasing the applied pressure (see Fig. S2), and formation or breaking down the hydrogen bonds between fluorine atoms on the edge pore and water molecules was not also affected by enhancing the applied pressure. Figure S2 shows changing the number of hydrogen bonds in the whole system that was approximately constant with changing the applied pressure.

3. 4. CONCLUSIONS

In this research, we performed the MD calculations to study the separation of AsO_3^{3-} ions, a significant pollutant of aqueous solutions, using the BNNS as a membrane. To this end, the hydrophilic pore was built and functionalized on the surface of a single-layer BNNS. This nanostructure sheet with a controllable size, desired charge state, and the ideal atomic structure was able to conduct water molecules through its pore with a high permeability, whereas AsO_3^{3-} ions were not able to pass through the pore. Not surprisingly, none of the AsO_3^{3-} ions could not pass through the pore even at high pressures. The aim of applying pressure in a wide range was to increase the number of water molecules passing through the pore. We found out all

essential factors in pore design, such as pore size (about 13.15 $Å^2$), and appropriate groups (F and H atoms) to passivate pore edge or designation form of pore area (higher hydrophilic), acting as a barrier. Finally, the results highlighted the successful performance of BNNS to separate the AsO_3^{3-} ions from an aqueous solution.

Conflict of Interest: The authors declare that they have no conflict of interest.

REFERENCES

[1] Srivastava, N. K.; Majumder, C. B., Novel biofiltration methods for the treatment of heavy metals from industrial wastewater. J. Hazard. Mater. **2008**, 151, 1-8. DOI: 10.1016/j.jhazmat.2007.09.101.

[2] Schneegurt, M. A.; Jain, J. C.; Menicucci, J. A.; Brown, S. A.; Kemner, K. M.; Garofalo, D. F.; Quallick, M. R.; Kulpa, C. F., Biomass byproducts for the remediation of wastewaters contaminated with toxic metals. *Environ. Sci. Technol.* **2001**, *35*, 3786-3791. DOI: 10.1021/es010766e.

[3] Sud, D.; Mahajan, G.; Kaur, M. P., Agricultural waste material as potential adsorbent for sequestering heavy metal ions from aqueous solutions -A review. *Bioresour. Technol.* **2008**, *99*, 6017-6027. DOI: 10.1016/j.biortech.2007.11.064.

[4] Monser, L.; Adhoum, N., Modified activated carbon for the removal of copper, zinc, chromium and cyanide from wastewater. *Sep. Purif. Technol.* **2002**, *26*, 137-146. DOI: 10.1016/S1383-5866(01)00155-1.

[5] Ratna Kumar, P.; Chaudhari, S.; Khilar, K. C.; Mahajan, S. P., Removal of arsenic from water by electrocoagulation. *Chemosphere* **2004**, *55*, 1245-1252. DOI: 10.1016/j.chemosphere.2003.12.025.

[6] Chen, O. -P.; Lin, Y. -J.; Cao, W. Z.; Chang, C. T., Arsenic removal with phosphorene and adsorption in solution. *Mater. Lett.* **2017**, *190*, 280-282. DOI: 10.1016/j.matlet.2017.01.030.

[7] Košutić, K.; Furač, L.; Sipos, L.; Kunst, B., Removal of arsenic and pesticides from drinking water by nanofiltration membranes. *Sep. Purif. Technol.* **2005**, *42*, 137-144. DOI:10.1016/j.seppur.2004.07.003.

[8] Srivastava, R.; Kommu, A.; Sinha, N.; Singh, J. K., Removal of arsenic ions using hexagonal boron nitride and graphene nanosheets: a molecular dynamics study. *Mol. Simul.* **2017**, *43*, 985-996. DOI: 10.1080/08927022.2017.1321754.

[9] Golberg, D.; Bando, Y.; Huang, Y.; Terao, T.; Mitome, M.; Tang, C.; Zhi, C., Boron Nitride Nanotubes and Nanosheets. ACS Nano 2010, 4, 2979-2993. DOI: 10.1021/nn1006495.

[10] Lei, W.; Portehault, D.; Liu, D.; Qin, S.; Chen, Y., Porous boron nitride nanosheets for effective water cleaning. Nat. Commun. 2013, 4, 1777. DOI: 10.1038/ncomms2818.

[11] Azamat, J.; Sattary, B. S.; Khataee, A.; Joo, S. W., Removal of a hazardous heavy metal from aqueous solution using functionalized graphene and boron nitride nanosheets: Insights from simulations. *J. Mol. Graphics Modell.* **2015**, *61*, 13-20. DOI: 10.1016/j.jmgm.2015.06.012.

[12] Chen, C.; Wang, J.; Liu, D.; Yang, C.; Liu, Y.; Ruoff, R. S.; Lei, W., Functionalized boron nitride membranes with ultrafast solvent transport performance for molecular separation. *Nat. Commun.* **2018**, *9*, 1902. DOI: 10.1038/s41467-018-04294-6.

[13] Jafarzadeh, R.; Azamat, J.; Erfan-Niya, H.; Hosseini, M., Molecular insights into effective water desalination through functionalized nanoporous boron nitride nanosheet membranes. *Appl. Surf. Sci.* **2019**, *471*, 921-928. DOI: 10.1016/j.apsusc.2018.12.069.

[14] Bangari, R. S.; Yadav, V. K.; Singh, J. K.; Sinha, N., Fe_3O_4-Functionalized boron nitride nanosheets as novel adsorbents for removal of arsenic(III) from contaminated water. *ACS Omega* **2020**, *5*, 10301-10314. DOI: 10.1021/acsomega.9b04295.

[15] Darvish Ganji, M.; Dodangeh, R., Hydrogen purification performance of a nanoporous hexagonal boron nitride membrane: molecular dynamics and first-principle simulations. *Phys. Chem. Chem. Phys.* **2017**, *19*, 12032-12044. DOI: 10.1039/c7cp01665d.

[16] Okada, S., Atomic configurations and energetics of vacancies in hexagonal boron nitride: First-principles total-energy calculations. *Physical Review B -Condensed Matter and Materials Physics* **2009**, *80*, 1-4. DOI: 10.1103/PhysRevB.80.161404.

[17] Schmidt, M. W.; Baldridge, K. K.; Boatz, J. A.;

Elbert, S. T.; Gordon, M. S.; Jensen, J. H.; Koseki, S.; Matsunaga, N.; Nguyen, K. A.; Su, S.; Windus, T. L.; Dupuis, M.; Montgomery, J. A., General atomic and molecular electronic structure system. *J. Comput. Chem.* **1993**, *14*, 1347-1363. DOI: 10.1002/jcc.540141112.

[18] Jorgensen, W. L.; Chandrasekhar, J.; Madura, J. D.; Impey, R. W.; Klein, M. L., Comparison of simple potential functions for simulating liquid water. *J. Chem. Phys.* **1983**, *79*, 926-935. DOI: 10.1063/1.445869.

[19] Vega, C.; Abascal, J. L., Simulating water with rigid non-polarizable models: a general perspective. *Phys. Chem. Chem. Phys.* **2011**, *13*, 19663-19688. DOI: 10.1039/c1cp22168j.

[20] Meng, X.; Huang, J., Enhancement of water flow across a carbon nanotube. *Mol. Simul.* **2016**, *42*, 215-219. DOI: 10.1080/08927022.2015.1034708.

[21] Brooks, B. R.; Bruccoleri, R. E.; Olafson, B. D.; States, D. J.; Swaminathan, S.; Karplus, M., CHARMM: A program for macromolecular energy, minimization, and dynamics calculations. *J. Comput. Chem.* **1983**, *4*, 187-217. DOI: 10.1002/jcc.540040211.

[22] Darden, T.; York, D.; Pedersen, L., Particle mesh Ewald: An N-log(N) method for Ewald sums in large systems. *J. Chem. Phys.* **1993**, *98*, 10089-10092. DOI: 10.1063/1.464397.

[23] Allen, M. P.; Tildesley, D. J., Computer Simulation of Liquids, Oxford University Press, 2017.

[24] Phillips, J. C.; Braun, R.; Wang, W.; Gumbart, J.; Tajkhorshid, E.; Villa, E.; Chipot, C.; Skeel, R. D.; Kalé, L.; Schulten, K., Scalable molecular dynamics with NAMD. *J. Comput. Chem.* 2005, *26*, 1781-1802. DOI: 10.1002/jcc.20289.

[25] Humphrey, W.; Dalke, A.; Schulten, K., VMD: Visual molecular dynamics. *J. Mol. Graphics* 1996, *14*, 33-38. DOI: 10.1016/0263-7855(96)00018-5.

[26] Cohen-Tanugi, D.; Grossman, J. C., Water permeability of nanoporous graphene at realistic pressures for reverse osmosis desalination. *J. Chem. Phys.* **2014**, 141, 074704. DOI: 10.1063/1.4892638

[27] Ludwig, R., Water: From Clusters to the Bulk. *Angew. Chem. Int. Ed.* **2001**, *40*, 1808-1827. DOI: 10.1002/1521-3773(20010518)40

[28] Mayne, C. G.; Saam, J.; Schulten, K.; Tajkhorshid, E.; Gumbart, J. C., Rapid parameterization of small molecules using the force field toolkit. *J. Comput. Chem.* **2013**, *34*, 2757-2770. DOI:10.1002/jcc.23422.

[29] Krekeler, C.; Site, L. D., Solvation of positive ions in water: the dominant role of water-water interaction. *J. Phys. Condens. Matter* **2007**, *19*. DOI: 10.1088/0953-8984/19/19/192101.